Mechanics and Quasi-Static Manipulation of Planar Elastic Kinematic Chains

Timothy Bretl, *Member, IEEE*, and Zoe McCarthy, *Student Member, IEEE*

***Abstract*—In this paper, we study quasi-static manipulation of a planar kinematic chain with a fixed base in which each joint is a linearly elastic torsional spring. The shape of this chain when in static equilibrium can be represented as the solution to a discrete-time optimal control problem, with boundary conditions that vary with the position and orientation of the last link. We prove that the set of all solutions to this problem is a smooth three-manifold that can be parameterized by a single chart. Empirical results in simulation show that straight-line paths in this chart are uniformly more likely to be feasible (as a function of distance) than straight-line paths in the space of boundary conditions. These results, which are consistent with an analysis of visibility properties, suggest that the chart we derive is a better choice of space in which to apply a sampling-based algorithm for manipulation planning. We describe such an algorithm and show that it is easy to implement.**

***Index Terms*—Deformable objects, manipulation planning, motion and path planning, optimal control.**

I. Introduction

CONSIDER a serial kinematic chain that moves in a planar workspace and that has a fixed base. Assume that each joint in this chain is a linearly elastic torsional spring and that the last link is held by a robotic gripper. The problem we address is to find a path of the gripper that causes the chain to move between given start and goal configurations, while remaining in static equilibrium and avoiding collision. This problem is a simple example of quasi-static manipulation planning in which the object to be manipulated is deformable.

What makes this problem seem hard is the apparent lack of coordinates to describe equilibrium configurations, i.e., configurations of the chain that would be in static equilibrium if the last link were held fixed by the gripper. The set of all equilibrium configurations has lower dimension than the configuration space of the chain; therefore, elements of this set cannot be found by rejection sampling. In addition, there are a countably infinite number of equilibrium configurations that correspond to a given placement of the gripper, none of which can be computed in closed form. For this reason, most of the literature on similar problems (see Section II) would suggest exploring the set of equilibrium configurations indirectly, by sampling placements of the gripper and using numerical simulation to find their effect on the chain. This approach was developed at length in the seminal work of Lamiraux and Kavraki [1], and was later applied by Moll and Kavraki [2] for the manipulation of elastic "deformable linear objects" like flexible wire, which can be viewed as a continuous analog of the chain we consider here. Our own work is really a direct extension of [2], where we look at a simpler finite-dimensional object (the chain) in order to develop the basis for an alternative approach.

Our contribution in this paper is to prove that the set of equilibrium configurations for a planar elastic kinematic chain is, in fact, a smooth manifold that can be parameterized explicitly by a single chart (see Section III). In other words, we will produce a finite set of coordinates that suffice to describe all possible configurations of the chain that can be achieved by quasi-static manipulation. The key idea is to express equilibrium configurations as local optima of a discrete-time optimal control problem. Rather than trying to compute solutions to this problem for given boundary conditions, we ask what must be satisfied by solutions to this problem for *any* boundary conditions. The coordinates we need are provided by costates that arise in necessary and sufficient conditions for optimality. Quasi-static manipulation planning becomes very easy if we work in the chart defined by these coordinates.

To justify this claim, we consider the benefits of applying a sampling-based planning algorithm in the chart we derive rather than in the space of boundary conditions (see Section IV). One benefit is related to the sampling strategy. Points in the chart we derive uniquely specify equilibrium configurations of the chain, which can be computed by evaluating a set of finite difference equations. Points in the space of boundary conditions do not uniquely specify equilibrium configurations—these depend on the entire path taken by the gripper and must be computed by solving a nonconvex optimization problem (e.g., using gradient descent). Another benefit is related to the local connection strategy. Empirical results in simulation show that straight-line paths in the chart we derive are uniformly more likely to be feasible (as a function of distance) than straight-line paths in the space of boundary conditions. These results are consistent with

Manuscript received April 3, 2012; revised August 25, 2012; accepted September 4, 2012. Date of publication October 9, 2012; date of current version February 1, 2013. This paper was recommended for publication by Associate Editor C. Torras and Editor B. J. Nelson upon evaluation of the reviewers' comments. This work was supported by the National Science Foundation under Grant CPS-0931871 and Grant CMMI-0956362.

T. Bretl is with the Department of Aerospace Engineering, University of Illinois at Urbana-Champaign, Urbana, IL 61801 USA (e-mail: tbretl@illinois.edu).

Z. McCarthy was with the Department of Electrical and Computer Engineering, University of Illinois at Urbana-Champaign, Urbana, IL 61801 USA. She is now with the Department of Electrical Engineering and Computer Sciences, University of California at Berkeley, Berkeley, CA 94720 USA (e-mail: mccarth4@illinois.edu).

This paper has supplementary downloadable material available at http://ieeexplore.ieee.org.

Color versions of one or more of the figures in this paper are available online at http://ieeexplore.ieee.org.

Digital Object Identifier 10.1109/TRO.2012.2218911

an analysis suggesting that the chart we derive has favorable visibility properties.

We are motivated in part by the wide variety of applications that require manipulation of deformable objects. Knot tying has been a particular focus of the robotics community because of its relevance to surgical suturing [3]–[8], but other applications of interest include cable routing [9], folding clothes [10]–[12], robotic origami [13], assembly of flexible circuit boards [14], surgical retraction of tissue [15], compliant parts handling [16]–[18], and the closely related fields of protein folding and geometric analysis of molecular motion [19]–[22]. We do not believe that a planar elastic kinematic chain is a good model of any "real-world" object found in these applications. We use it only to illustrate a new approach to manipulation planning. Our ongoing work suggests that this approach may generalize (see Section V).

We are also motivated by the link, which was pointed out by Tanner [23], between manipulation of deformable objects and control of hyper-redundant [24] and continuum [25]–[29] robots. These robots typically have many more degrees of freedom than are required to accomplish a given task. One approach to kinematic redundancy resolution is to choose a cost function and to restrict motion to the set of configurations that are locally optimal with respect to this cost function [30]. The robot then becomes a "deformable object" that is controlled by specifying the position and orientation of its end-effector. Our results show that it may be possible to parameterize the resulting set of locally optimal configurations. The coordinates we provide are an alternative to working either in the task space [31], [32] or in the space of modal shapes derived from a heuristic choice of basis functions [33]. Similar ideas have been applied to dynamic redundancy resolution [34], [35], and are related to the concept of operational space control [36].

The rest of this paper proceeds as follows. Section II gives an overview of related work. Our main result appears in Section III, where we characterize the set of equilibrium configurations for a planar elastic kinematic chain. We apply this result to manipulation planning in Section IV. We conclude with a brief discussion of future work in Section V, leaving proofs to the Appendix.

A preliminary version of this paper has appeared at a conference [37]. Two extensions are provided here, both related to the sampling-based algorithm used for manipulation planning in Section IV. First, we justify our choice of sampling strategy by giving a physical interpretation of the chart we derive (see Section III-B). Second, we justify our choice of local connection strategy with empirical results in simulation (see Section IV-B).

II. Related Work

There are two main approaches to manipulation planning for "deformable linear objects" like the chain we consider here: one that relies primarily on numerical simulation and another that uses task-based decomposition.

The first approach is exemplified by Moll and Kavraki [2], who provide a sampling-based planning algorithm for quasi-static manipulation of an inextensible elastic rod—as might be used to model a flexible wire or surgical thread—by robotic grippers in a 3-D workspace. Any framed curve traced by this rod when in static equilibrium is one that locally minimizes total elastic energy, which is defined as the integral of squared curvature plus squared torsion along the rod's entire length. The algorithm proceeds by sampling placements of each gripper and by using numerical methods to find minimal-energy curves that satisfy these boundary conditions. It measures distance between curves by the integral of the sum-squared difference in curvature and torsion, and connects nearby curves by spherical interpolation of gripper placement (i.e., by a local path in the space of boundary conditions), again using numerical methods to find the resulting path of the rod. The efficacy of this approach clearly derives from the choice of numerical methods. In [2], minimal-energy curves are approximated by recursive subdivision. Many other methods have been proposed (finite element, finite difference, etc.) that we will not mention here, since they are used for planning in much the same way. Current state of the art is perhaps the discrete geometric model of Bergou *et al.* [38], which has recently found application in robotics [39].

The second approach is exemplified by the work of Wakamatsu *et al.* [5] and of Saha and Isto [6] on knot tying with rope. Knot tying is an example of a manipulation task in which the goal is topological rather than geometric. It does not matter exactly what curve is traced by the rope, only that this curve has the correct sequence of crossings. Motion primitives can be designed to ensure that crossing operations are realizable by robotic grippers—in [5], these primitives rely on the rope being placed on a table and immobilized by gravity, while in [6], these primitives rely on fixtures (referred to as "needles" by analogy to knitting). This approach has been generalized to folding paper by Balkcom and Mason [13] and to folding clothes by van den Berg *et al.* [11]. "Crossings" are replaced by "folds," again realized either by relying on fixtures or on immobilization by gravity.

Like the first approach, we consider a geometric goal in this paper and model equilibrium configurations as local minima of total elastic energy. However, instead of relying on numerical simulation, we will derive coordinates that explicitly describe the set of all possible equilibrium configurations for our object of interest, a planar elastic kinematic chain. This result will allow us to plan a path *of the chain* through its set of equilibrium configurations—like the second approach—rather than plan indirectly by sampling placements of each gripper.

We have also been strongly influenced by prior analysis of the Kirchhoff elastic rod using calculus of variations and optimal control. This analysis has been done both from a Lagrangian [40], [41] and a Hamiltonian [42]–[46] perspective. It has led in some cases to global descriptions of extremal solutions (often called "solution manifolds") similar to what we derive in this paper. For example, Ivey and Singer [47] show that closed and quasiperiodic extremals of uniform, isotropic, linearly elastic rods are parameterized by a 2-D disk. Similarly, Neukirch and Henderson classify extremals of elastic rods with clamped boundary conditions [48] and apply numerical continuation to explicitly compute the set of all such extremals [49]. None of this work has been applied yet to manipulation

planning—Camarillo *et al.* [27] and Rucker *et al.* [28] are closest to making this link, in the context of continuum robots (e.g., tendon-driven or concentric tube).

In this discussion, we have omitted previous work that is not directly related to what we propose (e.g., fair curves and minimal-energy splines in computer graphics). See [2] or [50] for a broader overview. We emphasize that the planar elastic kinematic chain should not be viewed as a competing model to what appears in this other work. We chose it to illustrate our approach to manipulation planning because, as we will show in the following section, equilibrium configurations can be described as local optima of a discrete-time optimal control problem (as opposed to continuous-time)—this property allows us to rely on well-known necessary and sufficient conditions for optimality. Our approach has recently been extended to the Kirchhoff elastic rod [51], [52], and we hope it will further generalize to other continuous models like the Cosserat rod [53], which handles large deformation and allows both extension and shear.

III. Mechanics

In Section III-A, we fix notation and express equilibrium configurations of a planar elastic kinematic chain as local optima of a discrete-time optimal control problem. In Section III-B, we show that the set of configurations satisfying necessary conditions for local optimality is a smooth three-manifold that can be parameterized by a single chart (see Theorem 2), the coordinates of which have a simple interpretation as forces and torques. In Section III-C, we show that the set of configurations satisfying sufficient conditions for local optimality is an open subset of this manifold, and we provide an algorithm to test membership in this subset (see Theorem 4). Finally, in Section III-D, we define a "straight-line path" in both the manifold we derive and in the space of boundary conditions—this result is the basis for the local connection strategies we use for manipulation planning in Section IV.

A. Model

The kinematic chain in Fig. 1 moves in a planar workspace $\mathcal{W} = \mathbb{R}^2$. It has n revolute joints, where we assume $n > 3$. We index joints by $i \in \{0, \ldots, n-1\}$. The angle of each joint i is $u(i) \in \mathbb{R}$. We denote the entire sequence of joint angles by the function $u : \{0, \ldots, n-1\} \to \mathbb{R}$. We call the space of all possible u the joint space and identify it in the obvious way with $\mathcal{Q} = \mathbb{R}^n$. The chain has $n+1$ rigid links that we index by $i = \{0, \ldots, n\}$. We attach a coordinate frame to each link $1, \ldots, n$ so that the axis of joint $i-1$ passes through the origin of frame i. We attach a coordinate frame to link 0 so that the origin of frames 0 and 1 coincide. We describe the position and orientation of frame i relative to frame 0 by the homogenous transformation matrix

$$\begin{bmatrix} \cos x_3(i) & -\sin x_3(i) & x_1(i) \\ \sin x_3(i) & \cos x_3(i) & x_2(i) \\ 0 & 0 & 1 \end{bmatrix} \in SE(2)$$

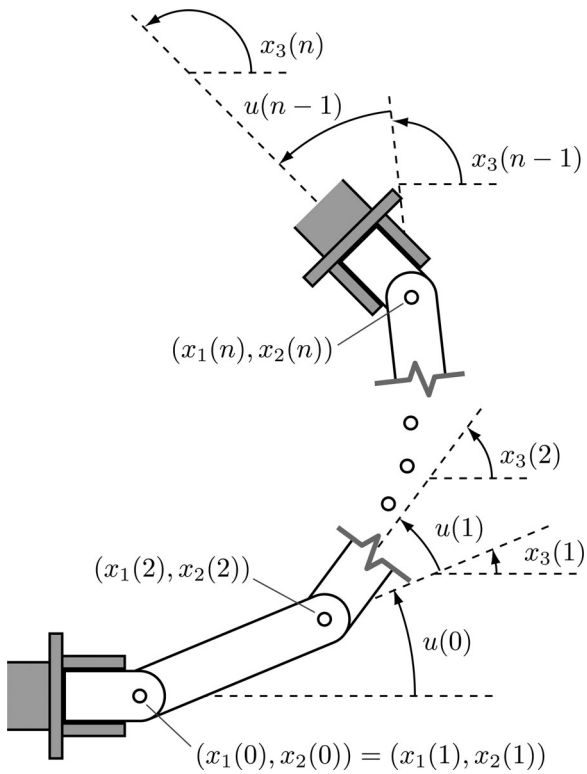

Fig. 1. Planar kinematic chain with n joints and $n+1$ rigid links that is held at each end by a robotic gripper. Each joint is a linearly elastic torsional spring. For a fixed position and orientation of each gripper, the chain relaxes to a shape that locally minimizes the energy in all n joints.

for some $x(i) \in \mathbb{R}^3$. Henceforth, we refer only to $x(i)$ and not to the element of $SE(2)$ to which $x(i)$ corresponds. This choice is for convenience and will cause no problems. It can be viewed as working in the chart $\mathbb{R}^2 \times (x_3(i) - \pi, x_3(i) + \pi]$, where equality in $x_3(i)$ is taken modulo 2π. We call $x(i)$ the state and call $\mathcal{X} = \mathbb{R}^3$ the state space. We specify $x(i)$ recursively with the finite difference equation

$$x(i+1) = x(i) + \begin{bmatrix} r_i \cos x_3(i) \\ r_i \sin x_3(i) \\ u(i) \end{bmatrix} \tag{1}$$

for $i \in \{0, \ldots, n-1\}$, where for convenience we choose

$$r_i = \begin{cases} 0, & \text{if } i = 0 \\ (n-1)^{-1}, & \text{otherwise} \end{cases}$$

so that the total length is 1. We denote the state trajectory by $x : \{0, \ldots, n\} \to \mathcal{X}$. Each end of the kinematic chain is held by a robotic gripper. We ignore the structure of these grippers, and simply assume that they fix arbitrary values of $x(0)$ and $x(n)$. We further assume, without loss of generality, that $x(0) = 0$. We call the space of all possible $x(n)$ the task space and denote it by $\mathcal{B} \subset \mathbb{R}^3$. Again, the reader should think of each $b \in \mathcal{B}$ as belonging to a chart of $SE(2)$, where equality in b_3 is taken modulo 2π.

Finally, we assume that each joint i in the kinematic chain is a linearly elastic torsional spring with unit modulus and, therefore, has potential energy $u(i)^2/2$. For fixed endpoints, the chain will

remain motionless only if its shape locally minimizes the total energy in all n joints. In particular, we say that (u, x) is in static equilibrium if it is a locally optimal solution to

$$\begin{aligned} \underset{\substack{u \in \mathcal{Q} \\ x(0), \ldots, x(n) \in \mathcal{X}}}{\text{minimize}} \quad & \frac{1}{2}\sum_{i=0}^{n-1} u(i)^2 \\ \text{subject to} \quad & x(i+1) = x(i) + \begin{bmatrix} r_i \cos x_3(i) \\ r_i \sin x_3(i) \\ u(i) \end{bmatrix} \\ & \qquad \text{for all } i \in \{0, \ldots, n-1\} \\ & x(0) = 0 \\ & x(n) = b \end{aligned} \tag{2}$$

for some $b \in \mathcal{B}$. We note that, in this discrete-time optimal control problem, the "time step" i is used to index joints.

For quasi-static manipulation, we will require that (u, x) is nonsingular as well as in static equilibrium. The reason for this requirement is that singularities will turn out to be configurations at which there is ambiguity in how the chain responds to motion of each gripper. We will treat this requirement as an assumption in Section III-B and will make it precise in Section III-C (as Theorem 5). Note that (u, x) is nonsingular if and only if it is regular with respect to the constraints in (2), since these constraints are exactly the forward kinematic relations. Following the literature on equality-constrained minimization [54], we will use the term "regular" in our analysis of (2).

B. Necessary Conditions for Static Equilibrium

The following theorem is an application of first-order necessary conditions for equality-constrained minimization to the problem (2), similar to [55, Ch. 2.6].

Theorem 1: If (u, x) is both regular and a local optimum of (2), then there exists a costate trajectory

$$p : \{0, \ldots, n\} \to \mathbb{R}^3$$

that satisfies

$$p(i)^T = \nabla_{x(i)} H\left(x(i), p(i+1), u(i)\right) \tag{3}$$

$$0 = \nabla_{u(i)} H\left(x(i), p(i+1), u(i)\right) \tag{4}$$

for all $i \in \{0, \ldots, n-1\}$, where

$$\begin{aligned} H\left(x(i), p(i+1), u(i)\right) = {} & \frac{1}{2}u(i)^2 \\ & + p_1(i+1)\left(x_1(i) + r_i \cos x_3(i)\right) \\ & + p_2(i+1)\left(x_2(i) + r_i \sin x_3(i)\right) \\ & + p_3(i+1)\left(x_3(i) + u(i)\right) \end{aligned}$$

is the Hamiltonian function.

Proof: See [54, Ch. 11.3]. ∎

Theorem 1 provides a set of candidates for local optimality of (2), which we will proceed to characterize. Let

$$\mathcal{C} \subset \mathbb{R}^n \times \mathbb{R}^{3(n+1)}$$

be the set of all regular (u, x) for which there exists p satisfying (3) and (4). We will show that $\mathcal{C}$ is a smooth three-manifold. In particular, (3) and (4) require that

$$\begin{aligned} p(i)^T &= p(i+1)^T J_i \\ u(i) &= -p(i+1)^T e_3 \end{aligned}$$

for $i \in \{0, \ldots, n-1\}$, where

$$J_i = \begin{bmatrix} 1 & 0 & -r_i \sin x_3(i) \\ 0 & 1 & r_i \cos x_3(i) \\ 0 & 0 & 1 \end{bmatrix} \quad \text{and} \quad e_3 = \begin{bmatrix} 0 \\ 0 \\ 1 \end{bmatrix}.$$

The inverse

$$J_i^{-1} = \begin{bmatrix} 1 & 0 & r_i \sin x_3(i) \\ 0 & 1 & -r_i \cos x_3(i) \\ 0 & 0 & 1 \end{bmatrix}$$

exists everywhere. Hence, (u, x) and p are related by the finite difference equations

$$\begin{aligned} u(i) &= -p(i)^T J_i^{-1} e_3 \\ x(i+1) &= x(i) + \begin{bmatrix} r_i \cos x_3(i) \\ r_i \sin x_3(i) \\ u(i) \end{bmatrix} \\ p(i+1) &= (J_i^{-1})^T p(i) \end{aligned} \tag{5}$$

for $i \in \{0, \ldots, n-1\}$. Recalling that $x(0) = 0$, we see that (5) is completely defined by the choice of $p(0)$. For $a \in \mathbb{R}^3$, let $p(0) = a$, and compute (u, x) and p according to (5). Denote the resulting map by

$$\Psi(a) = (u, x) \tag{6}$$

$$\Gamma(a) = p. \tag{7}$$

By construction, $\Psi(a)$ and $\Gamma(a)$ satisfy (3) and (4) for all $a \in \mathbb{R}^3$. However, $\Psi(a)$ is regular only for certain choices of a. In particular, define

$$\mathcal{A} = \mathbb{R}^3 \setminus \mathcal{S}$$

where

$$\mathcal{S} = \left\{ \begin{bmatrix} h \\ k(n-1)\pi \\ l\pi \end{bmatrix} \in \mathbb{R}^3 : h \in \mathbb{R} \text{ and } k, l \in \mathbb{Z} \right\}.$$

We show in Appendix B that $\Psi(a)$ is regular if and only if $a \in \mathcal{A}$ (see Lemma 7). This result implies that $\Psi : \mathcal{A} \to \mathcal{C}$ is a homeomorphism (see Lemma 9), and allows us to draw the following conclusion.

Theorem 2: $\mathcal{C}$ is a smooth three-manifold with smooth structure that is determined by an atlas with the single chart $(\mathcal{C}, \Psi^{-1})$.

Proof: Since Ψ is a homeomorphism by Lemma 9 (see Appendix B) and $\mathcal{A} \subset \mathbb{R}^3$ is open, then $(\mathcal{C}, \Psi^{-1})$ is a chart whose domain covers $\mathcal{C}$. Our result is an immediate consequence of Lemma 3 (see Appendix A). ∎

As a corollary, we know that $\mathcal{A}$ is also a smooth three-manifold and that $\Psi : \mathcal{A} \to \mathcal{C}$ is, in fact, a diffeomorphism.

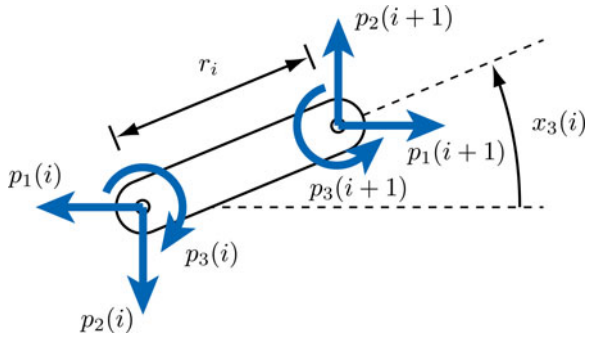

Fig. 2. Forces and torques applied to link i of the planar elastic kinematic chain, providing a physical interpretation of the costate trajectory.

We emphasize that the dimensionality of $\mathcal{A}$ does not increase with the number of joints n. We find this result somewhat remarkable, because it means that the complexity of manipulation planning (see Section IV) does not scale as it normally would. In hindsight, there are two reasons why we might have expected this result. First, since any quasi-static motion of the chain is caused by motion of the gripper, and since the configuration of the gripper lives in $SE(2)$, we conclude that the set of equilibrium configurations must—at least locally—have dimension three. Second, the principle of virtual work [56] requires satisfaction of

$$\mathbf{J}(\theta)^T f = -\theta \tag{8}$$

in static equilibrium, where

$$\theta = \begin{bmatrix} u(0) & \cdots & u(n-1) \end{bmatrix}^T \in \mathbb{R}^n$$

is the vector of joint angles, $\mathbf{J}(\theta) \in \mathbb{R}^{3\times n}$ is the manipulator Jacobian, and $f \in \mathbb{R}^3$ is the force and torque applied by the gripper on link n. The implicit function theorem tells us that nonsingular solutions to (8) are locally parameterized by f, which again has dimension three.

Before proceeding, we also note another way to derive the finite difference equations (5) that gives a physical interpretation of the costate trajectory. For $i \in \{0, \ldots, n-1\}$, let us simply define $(p_1(i+1), p_2(i+1))$ as the force on link i due to joint i, and similarly $p_3(i+1)$ as the torque on link i due to joint i, written in the coordinates of frame 0. These forces and torques are transmitted from link to link by torsional springs of unit modulus. Hence, it is clear both that $-p(i)$ describes the force and torque on link i due to joint $i-1$ and that $u(i) = -p_3(i+1)$ for all $i \in \{0, \ldots, n-1\}$. From a force and torque balance (see Fig. 2), we have

$$\begin{aligned} p_1(i+1) &= p_1(i) \\ p_2(i+1) &= p_2(i) \\ p_3(i+1) &= p_3(i) + p_1(i) r_i \sin x_3(i) - p_2(i) r_i \cos x_3(i) \end{aligned}$$

exactly as in (5). In particular, if the chain is in static equilibrium and is not in singularity, then its configuration is uniquely defined by the force and torque $p(0)$ at the fixed base, i.e., by the choice of $a \in \mathcal{A}$. Singularities of the chain are exactly those configurations at which a is indeterminate. This relationship between forces and torques and the costate trajectory p (which is nothing more than a collection of Lagrange multipliers) is entirely classical [50]. We will use it in Section IV-A to justify our choice of sampling strategy for manipulation planning.

C. Sufficient Conditions for Static Equilibrium

Given $(u, x) = \Psi(a)$ and $p = \Gamma(a)$ for $a \in \mathcal{A}$, we compute

$$\begin{aligned} \nabla^2_{u(i)u(i)} H\left(x(i), p(i+1), u(i)\right) &= 1 \\ \nabla^2_{u(i)x(i)} H\left(x(i), p(i+1), u(i)\right) &= \begin{bmatrix} 0 & 0 & 0 \end{bmatrix} \\ \nabla^2_{x(i)x(i)} H\left(x(i), p(i+1), u(i)\right) &= Q_i \end{aligned}$$

for $i \in \{0, \ldots, n-1\}$, where

$$Q_i = \begin{bmatrix} 0 & 0 & 0 \\ 0 & 0 & 0 \\ 0 & 0 & -r_i\left(a_1 \cos x_3(i) + a_2 \sin x_3(i)\right) \end{bmatrix}.$$

We use $\delta u \in T\mathcal{Q}$ and $\delta x(0), \ldots, \delta x(n) \in T\mathcal{X}$ to denote perturbations of the input and state trajectory, where in this case $T\mathcal{Q}$ and $T\mathcal{X}$ may be identified with $\mathcal{Q}$ and $\mathcal{X}$, respectively. The following theorem is an application of second-order sufficiency conditions for equality-constrained minimization, similar to [55, Ch. 2.6]:

Theorem 3: Let $(u, x) = \Psi(a)$ and $p = \Gamma(a)$ for $a \in \mathcal{A}$. If $(\delta u, \delta x) = (0, 0)$ is the unique solution to

$$\begin{aligned} \underset{\substack{\delta u \in T\mathcal{Q} \\ \delta x(0), \ldots, \delta x(n) \in T\mathcal{X}}}{\text{minimize}} \quad & \frac{1}{2}\sum_{i=0}^{n-1} \left(\delta x(i)^T Q_i \delta x(i) + \delta u(i)^2\right) \\ \text{subject to} \quad & \delta x(i+1) = J_i \delta x(i) + e_3 \delta u(i) \\ & \qquad \text{for all } i \in \{0, \ldots, n-1\} \\ & \delta x(0) = 0 \\ & \delta x(n) = 0 \end{aligned} \tag{9}$$

then (u, x) is a local optimum of (2) for $b = x(n)$.

Proof: See [54, Ch. 11.5]. ∎

Theorem 3 allows us to say which points $a \in \mathcal{A}$ actually produce local optima $\Psi(a) \in \mathcal{C}$ of (2). In particular, let

$$\mathcal{A}_{\text{stable}} \subset \mathcal{A}$$

be the set of all a for which $(\delta u, \delta x) = (0, 0)$ is the unique solution to (9), and let

$$\mathcal{C}_{\text{stable}} = \Psi(\mathcal{A}_{\text{stable}}) \subset \mathcal{C}.$$

The following result establishes correctness of IsStable (see Fig. 3), which tests membership in $\mathcal{A}_{\text{stable}}$.

Theorem 4: The point $a \in \mathcal{A}$ is an element of $\mathcal{A}_{\text{stable}}$ if and only if IsStable(a) returns TRUE.

Proof: See Appendix C. ∎

Another important consequence of membership in $\mathcal{A}_{\text{stable}}$ is smooth local dependence of (2) on variation in b. Define

$$\mathcal{B}_{\text{stable}} = \{x(n) \in \mathcal{B} : (u, x) \in \mathcal{C}_{\text{stable}}\}$$

ISSTABLE(a)

Given $a \in \mathcal{A}$, do the following:

- Compute $(u, x) = \Psi(a)$ and $p = \Gamma(a)$.
- Compute

$$A = \begin{bmatrix} e_3 & 0 & 0 & 0 & -I & 0 & 0 \\ 0 & e_3 & 0 & 0 & J_{n-3} & -I & 0 \\ 0 & 0 & e_3 & 0 & 0 & J_{n-2} & -I \\ 0 & 0 & 0 & e_3 & 0 & 0 & J_{n-1} \end{bmatrix}$$

$$B = \begin{bmatrix} -J_{n-4} & 0 & 0 & 0 \end{bmatrix}^T$$

$$M = \begin{bmatrix} I & 0 & 0 & 0 \\ 0 & Q_{n-3} & 0 & 0 \\ 0 & 0 & Q_{n-2} & 0 \\ 0 & 0 & 0 & Q_{n-1} \end{bmatrix},$$

and find a basis N for the null space of A. If

$$N^T M N > 0$$

then take

$$A^\dagger = A^T (A A^T)^{-1}$$
$$K = (N^T M N)^{-1} N^T M$$
$$P_{n-4} = Q_{n-4} + (A^\dagger B)^T (I - NK)^T M (I - NK)(A^\dagger B),$$

otherwise return FALSE.

- For each $i \in \{n-5, \ldots, 0\}$, if

$$s_{i+1} = 1 + e_3^T P_{i+1} e_3 > 0$$

then take

$$P_i = Q_i + J_i^T (P_{i+1} - P_{i+1} e_3 s_{i+1}^{-1} e_3^T P_{i+1}) J_i,$$

otherwise return FALSE.

Return TRUE.

Fig. 3. Algorithm that checks the membership of a in $\mathcal{A}_{\text{stable}} \subset \mathcal{A}$.

and let $\Phi : \mathcal{C} \to \mathcal{B}$ be the map taking (u, x) to $x(n)$. We note that $\mathcal{A}_{\text{stable}}$ is open, hence that

$$\Psi|_{\mathcal{A}_{\text{stable}}} : \mathcal{A}_{\text{stable}} \to \mathcal{C}_{\text{stable}}$$

is a diffeomorphism. The following theorem is then an application of sensitivity analysis to equality-constrained minimization, similar to [55, Ch. 6.10–6.11]:

Theorem 5: The map

$$\Phi \circ \Psi|_{\mathcal{A}_{\text{stable}}} : \mathcal{A}_{\text{stable}} \to \mathcal{B}_{\text{stable}}$$

is a local diffeomorphism.

Proof: See [54, Ch. 11.7]. ∎

D. Straight-Line Paths

In what follows, we require the computation of "straight-line paths" in both $\mathcal{A}$ and $\mathcal{B}$. Let $a_{\text{start}}, a_{\text{goal}} \in \mathcal{A}_{\text{stable}}$. We will say that a_{start} and a_{goal} are *$\mathcal{A}$-connected* if

$$a_{\text{start}} + t\,(a_{\text{goal}} - a_{\text{start}}) \in \mathcal{A}_{\text{stable}}$$

for $t \in [0, 1]$. It is equivalent to say that a_{start} and a_{goal} are connected by a straight-line path in $\mathcal{A}_{\text{stable}}$. In order to define the appropriate notion of *$\mathcal{B}$-connected*, we first provide a recursive formula to compute $\nabla_a (\Phi \circ \Psi|_{\mathcal{A}_{\text{stable}}})$. Given $(u, x) = \Psi(a)$ and $p = \Gamma(a)$ for $a \in \mathcal{A}$, we apply Lemma 4 (see Appendix B) to rewrite (5) as

$$\begin{aligned} x_1(i+1) &= x_1(i) + r_i \cos x_3(i) \\ x_2(i+1) &= x_2(i) + r_i \sin x_3(i) \\ x_3(i+1) &= x_3(i) - a_1 \left(x_2(i) + r_i \sin x_3(i)\right) \\ &\quad + a_2 \left(x_1(i) + r_i \cos x_3(i)\right) - a_3. \end{aligned}$$

Taking the gradient of both sides with respect to a, we find that the matrix $D(i) \in \mathbb{R}^{3\times 3}$ with entries

$$[D(i)]_{jk} = \frac{\partial x_j(i)}{\partial a_k}$$

satisfies the update rule

$$D(i+1) = F(i) D(i) + G(i) \tag{10}$$

where

$$F(i) = \begin{bmatrix} 1 & 0 & -r_i \sin x_3(i) \\ 0 & 1 & r_i \cos x_3(i) \\ a_2 & -a_1 & 1 - r_i \left(a_1 \cos x_3(i) + a_2 \sin x_3(i)\right) \end{bmatrix}$$

$$G(i) = \begin{bmatrix} 0 & 0 & 0 \\ 0 & 0 & 0 \\ -x_2(i) - r_i \sin x_3(i) & x_1(i) + r_i \cos x_3(i) & -1 \end{bmatrix}.$$

Evaluating (10) for $i \in \{0, \ldots, n-1\}$ with initial condition $D(0) = 0$ produces $\nabla_a (\Phi \circ \Psi|_{\mathcal{A}_{\text{stable}}}) = D(n)$. Now, let

$$b_{\text{start}} = \Phi \circ \Psi|_{\mathcal{A}_{\text{stable}}}(a_{\text{start}}) \quad \text{and} \quad b_{\text{goal}} = \Phi \circ \Psi|_{\mathcal{A}_{\text{stable}}}(a_{\text{goal}}).$$

Define $\beta : [0, 1] \to \mathcal{B}$ by

$$\beta(t) = b_{\text{start}} + t\,(b_{\text{goal}} - b_{\text{start}})$$

where the angular difference is taken modulo 2π and restricted to $(-\pi, \pi]$ as usual. Assume that $\beta(t) \in \mathcal{B}_{\text{stable}}$ for all $t \in [0, 1]$. Let $\alpha : [0, 1] \to \mathcal{A}$ be the solution to

$$\dot{\alpha}(t) = \left(\nabla_a (\Phi \circ \Psi|_{\mathcal{A}_{\text{stable}}})\big|_{a=\alpha(t)}\right)^{-1} (b_{\text{goal}} - b_{\text{start}}) \tag{11}$$

with the initial condition $\alpha(0) = a_{\text{start}}$. We know that this solution exists and is unique because $\Phi \circ \Psi|_{\mathcal{A}_{\text{stable}}}$ is a local diffeomorphism. Then, by construction, we have

$$\beta(t) = \Phi \circ \Psi|_{\mathcal{A}_{\text{stable}}} \circ \alpha(t)$$

for $t \in [0, 1]$. Note that, because $\Phi \circ \Psi|_{\mathcal{A}_{\text{stable}}}$ is only a local diffeomorphism, this result does not necessarily imply that $\alpha(1) = a_{\text{goal}}$. We will say that a_{start} and a_{goal} are *$\mathcal{B}$-connected* if indeed $\alpha(1) = a_{\text{goal}}$ and if our assumption that $\beta(t) \in \mathcal{B}_{\text{stable}}$ for $t \in [0, 1]$ was correct. We will use our definition of $\mathcal{A}$-connected and $\mathcal{B}$-connected as local connection strategies in the sampling-based planning algorithm in Section IV-A.

IV. QUASI-STATIC MANIPULATION

The results of Section III make it clear how to do quasi-static manipulation planning for the planar elastic kinematic chain in

Fig. 1. Recall that we want to find a path of the gripper that causes the chain to move between given start and goal configurations, while remaining in static equilibrium. As pointed out by Lamiraux and Kavraki [1], it is equivalent to finding a path *of the chain* through its set of equilibrium configurations. What makes this problem seem hard is the apparent lack of coordinates to describe these equilibrium configurations. Section III gives us the coordinates we need.

In particular, we showed that any equilibrium configuration can be represented by a point in the open subset $\mathcal{A}_{\text{stable}} \subset \mathcal{A} \subset \mathbb{R}^3$. It is entirely correct to think of $\mathcal{A}$ as the "configuration space" of the chain during quasi-static manipulation, and to think of $\mathcal{A}_{\text{stable}}$ as the "free space." Theorem 2 tells us how to map points in $\mathcal{A}$ to configurations of the chain. Theorem 4 tells us how to test membership in $\mathcal{A}_{\text{stable}}$, i.e., it gives us a "collision checker." Finally, Theorem 5 tells us that paths in $\mathcal{A}_{\text{stable}}$ can be "implemented" by the robotic gripper by establishing a well-defined map between differential changes in the shape of the chain (represented by $\mathcal{A}_{\text{stable}}$) and in the placement of the gripper (represented by $\mathcal{B}_{\text{stable}}$).

In other words, we have expressed the quasi-static manipulation planning problem for planar elastic kinematic chains as a standard motion planning problem in a configuration space of dimension three, for which there are hundreds of possible solution approaches [57]–[59].

In Section IV-A, we present one solution approach based on the use of a sampling-based planning algorithm. In Section IV-B, we compare this approach with what was suggested by the representative work of Moll and Kavraki [2]. Finally, in Section IV-C, we reconsider our choice of coordinates in light of concerns about the sensitivity of $\Psi : \mathcal{A} \to \mathcal{C}$ to perturbation.

A. Sampling-Based Planning Algorithm

Here is one way to implement a sampling-based algorithm, such as probabilistic roadmap planning [60], for quasi-static manipulation planning:

- Sample points uniformly at random in
$$\{a \in \mathcal{A} : \|a\|_\infty \leq w\}$$
where w is an upper bound on allowable forces (a_1, a_2) and torques a_3 at the base of the chain (see Section III-B).
- Add each point a as a node to the roadmap if the function IsStable(a) returns TRUE (see Section III-C).
- Add an edge between each pair of nodes a and a' if they are $\mathcal{A}$-connected (see Section III-D). This test can be approximated as usual by sampling points along the straight-line path from a to a' at some resolution, evaluating IsStable at each point.
- Declare $a_{\text{start}}, a_{\text{goal}} \in \mathcal{A}_{\text{stable}}$ to be path-connected if they are connected by a sequence of nodes and edges in the roadmap. This sequence is a continuous and piecewise-smooth map
$$\alpha : [0, 1] \to \mathcal{A}_{\text{stable}}$$
where $\alpha(0) = a_{\text{start}}$, and $\alpha(1) = a_{\text{goal}}$.
- Move the robotic gripper along the path
$$\Phi \circ \Psi|_{\mathcal{A}_{\text{stable}}} \circ \alpha : [0, 1] \to \mathcal{B}_{\text{stable}}.$$
This path is again continuous and piecewise-smooth, and can be evaluated at waypoints $t \in [0, 1]$ by solving the finite difference equations (5).

Each step is trivial to implement using modern numerical methods. It is also easy to include other constraints, such as self-collision, within this basic framework.

B. Analysis and Experimental Results

The overall structure of the algorithm in Section IV-A is exactly as suggested by Moll and Kavraki [2]. The key difference here is the choice of sampling and local connection strategies, and, particularly, the choice of *space* in which to implement these strategies. Instead of computing samples and straight-line paths in $\mathcal{B}$ (boundary conditions), we compute them in $\mathcal{A}$ (equilibrium configurations), which is something we can do only because of the analysis provided in Section III.

One advantage of this choice is that points in $\mathcal{A}$ uniquely specify equilibrium configurations of the chain, which can be computed by evaluating the finite difference equations (5). Points in $\mathcal{B}$ do not uniquely specify equilibrium configurations, which in this case depend on a_{start} and on the entire path
$$\beta : [0, 1] \to \mathcal{B}$$
taken by the gripper and must be computed by solving a differential equation similar to (11). Indeed, we emphasize that "start" and "goal" for manipulation planning must be points in $\mathcal{A}_{\text{stable}}$, or equivalently points in $\mathcal{C}_{\text{stable}}$ through the diffeomorphism Ψ. It is insufficient to specify start and goal by points in $\mathcal{B}_{\text{stable}}$. We note further that planning heuristics like lazy collision-checking [61]—which bring huge speedups in practice—are easy to apply when planning in $\mathcal{A}$ but hard to apply when planning in $\mathcal{B}$.

A second advantage of our choice to work in $\mathcal{A}$ is that straight-line paths in $\mathcal{A}$ are uniformly more likely to be feasible (as a function of distance) than straight-line paths in $\mathcal{B}$. As a consequence, we expect that fewer nodes will be required by a sampling-based planner to capture the connectivity of $\mathcal{A}_{\text{stable}}$ [58], [59]. Before presenting empirical results that justify this claim, we will discuss why it might be true.

Consider the four-joint chain in Fig. 4. If we restrict $|u(i)| \leq \pi$, then there are at most two inverse kinematic solutions for any given $u(0)$; therefore, it is possible to visualize the energy landscape and to see the local minima. Fig. 4, in particular, shows three different equilibrium configurations associated with the same boundary conditions. Each one corresponds to a local minimum of potential energy. In addition, snapshots of quasi-static manipulation for a particular choice of a_{start} and a_{goal} are shown. In this case, a_{start} and a_{goal} are $\mathcal{A}$-connected. Therefore, the algorithm in Section IV-A produces a single straight-line path in $\mathcal{A}_{\text{stable}}$. This path is implemented by moving the gripper along the path
$$\Phi \circ \Psi|_{\mathcal{A}_{\text{stable}}} \circ \alpha : [0, 1] \to \mathcal{B}$$

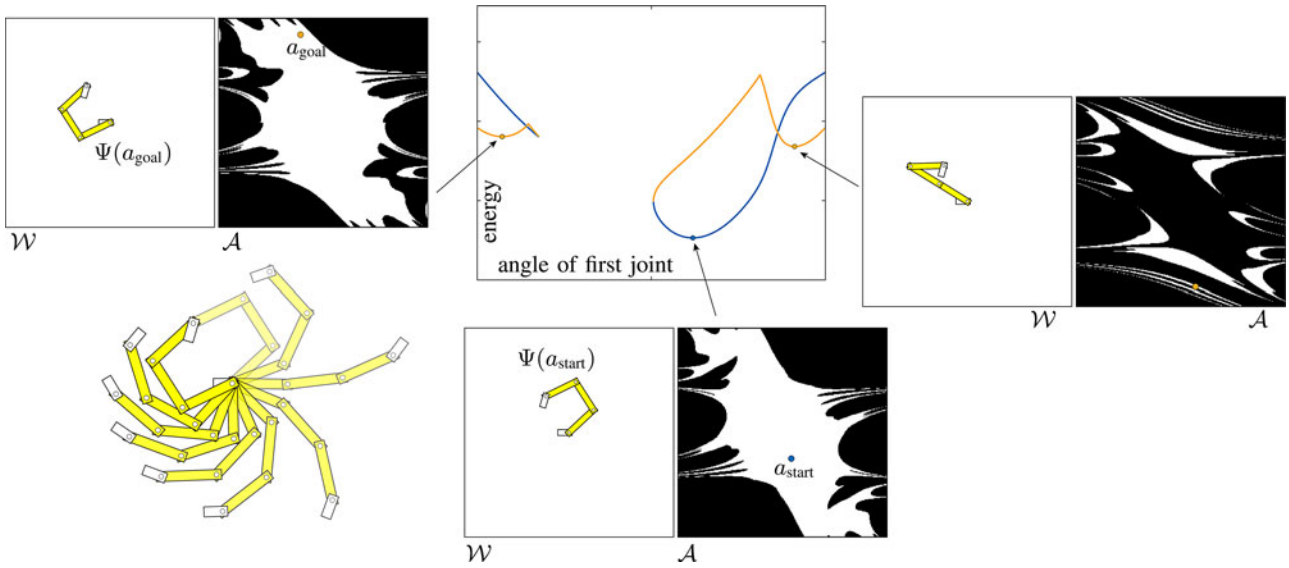

Fig. 4. Three equilibrium configurations of a four-joint elastic kinematic chain for fixed boundary conditions. Each one corresponds to a local minimum of potential energy, i.e., to a local optimum of (2). We show the point $a \in \mathcal{A}$ and the configuration $\Psi(a) \in \mathcal{C}$ associated with each local minimum. We are showing only a slice of $\mathcal{A}$ for fixed a_1 in each case—the nonshaded part of this slice is in $\mathcal{A}_{\text{stable}}$. Note that the configuration at upper right is nonsingular. Snapshots of quasi-static manipulation from $\Psi(a_{\text{start}})$ to $\Psi(a_{\text{goal}})$— which are given by a straight-line path from a_{start} to a_{goal}—are shown at lower left. In this example, the first link is held fixed, and we imagine that a robotic gripper is changing the position and orientation of the last link. The energy landscape, of course, varies along this path (see multimedia attachment as supplementary material).

in $\mathcal{B}_{\text{stable}}$, where

$$\alpha(t) = a_{\text{start}} + t\,(a_{\text{goal}} - a_{\text{start}})\,.$$

It is interesting to consider what would have happened if we had tried to plan a path from a_{start} to a_{goal} by working in the task space $\mathcal{B}$ rather than in the space $\mathcal{A}$ of equilibrium configurations. Clearly, the resulting plan cannot be represented by a single straight line in $\mathcal{B}$. We have

$$b_{\text{start}} = \Phi \circ \Psi|_{\mathcal{A}_{\text{stable}}}(a_{\text{start}}) = \Phi \circ \Psi|_{\mathcal{A}_{\text{stable}}}(a_{\text{goal}}) = b_{\text{goal}}$$

in this case (recalling that equality in orientation is taken modulo 2π); therefore, (11) results in zero motion—i.e., a_{start} and a_{goal} are not $\mathcal{B}$-connected. In the language of sampling-based planning [58]–[60], we say that a_{goal} is visible from a_{start} when using a straight-line local connection strategy in $\mathcal{A}$, but is not visible when using the analogous strategy in $\mathcal{B}$.

We can generalize this example as follows.

Lemma 1: If $a, a' \in \mathcal{A}_{\text{stable}}$ are $\mathcal{B}$-connected and $a \neq a'$, then $\Phi \circ \Psi|_{\mathcal{A}_{\text{stable}}}(a) \neq \Phi \circ \Psi|_{\mathcal{A}_{\text{stable}}}(a')$.

Proof: Assume to the contrary that

$$b = \Phi \circ \Psi|_{\mathcal{A}_{\text{stable}}}(a) = \Phi \circ \Psi|_{\mathcal{A}_{\text{stable}}}(a') = b'.$$

Then, the straight-line path from b to b' results in zero motion; therefore, we must have had $a = a'$, which is a contradiction. ■

As a corollary, we can prove an even stronger result.

Lemma 2: Let $a, a' a'' \in \mathcal{A}_{\text{stable}}$. Assume that $a \neq a'$ and $\Phi \circ \Psi|_{\mathcal{A}_{\text{stable}}}(a) = \Phi \circ \Psi|_{\mathcal{A}_{\text{stable}}}(a')$. If a and a'' are $\mathcal{B}$-connected, then a' and a'' are not $\mathcal{B}$-connected.

Proof: First, consider the case $a = a''$. We have $a' \neq a''$ by assumption; therefore, Lemma 1 implies that a' and a'' are not $\mathcal{B}$-connected. Now, consider the case $a \neq a''$. Define $a_{\text{start}} = a''$. Since $\Phi \circ \Psi|_{\mathcal{A}_{\text{stable}}}(a) = \Phi \circ \Psi|_{\mathcal{A}_{\text{stable}}}(a')$, the path $\alpha : [0, 1] \to \mathcal{A}$ produced by (11) is the same regardless of whether $a_{\text{goal}} = a$ or $a_{\text{goal}} = a'$. In particular, since both $a \neq a'$ and $\alpha(1) = a$ by assumption, we must have $\alpha(1) \neq a'$. Therefore, by definition, a' and a'' are not $\mathcal{B}$-connected. ■

Lemma 2 implies that no fewer than three "straight-line paths" in $\mathcal{B}_{\text{stable}}$ are required to connect two different equilibrium configurations that share the same boundary conditions. No such restriction exists on connections made in $\mathcal{A}_{\text{stable}}$, strongly suggesting that $\mathcal{A}_{\text{stable}}$ has favorable visibility properties (in general) compared with $\mathcal{B}_{\text{stable}}$.

Fig. 5 shows experimental results that support this claim for a chain with $n = 4$ joints and with $n = 10$ joints. In each case, 20 000 pairs of points $a, a' \in \mathcal{A}_{\text{stable}}$ were generated by sampling uniformly at random in

$$\{a \in \mathcal{A} : |a_1| < 100, |a_2| < 100, |a_3| < \pi\}$$

and rejecting points that were not in $\mathcal{A}_{\text{stable}}$. We tested whether each pair of points was $\mathcal{A}$-connected and $\mathcal{B}$-connected (as in Section III-D), including joint limits (restricting $|u(i)| < \pi$ for $i \in \{0, \ldots, n-1\}$) and self-collision as well as stability constraints. We computed the probability that each type of connection was successful as a function of Euclidean distance in $\mathcal{A}$, $\mathcal{B}$, and $\mathcal{Q}$. Fig. 5 shows that $\mathcal{A}$-connection was, in general, uniformly more likely to be successful as a function of distance than $\mathcal{B}$-connection. This result held regardless of the measure used for distance. The only apparent exception to this result in our experiments was for $n = 4$ as distance in $\mathcal{A}$ grew higher than 20. However, note that—as shown by the histogram in Fig. 5—this case also corresponded to very low counts in the number of sample pairs, exactly where we might expect to see higher variance in our results.

Given that similar results were obtained for a chain with $n = 4$ joints and $n = 10$ joints in Fig. 5, it is natural to wonder if there was a corresponding similarity in the shape of $\mathcal{A}_{\text{stable}}$. In fact,

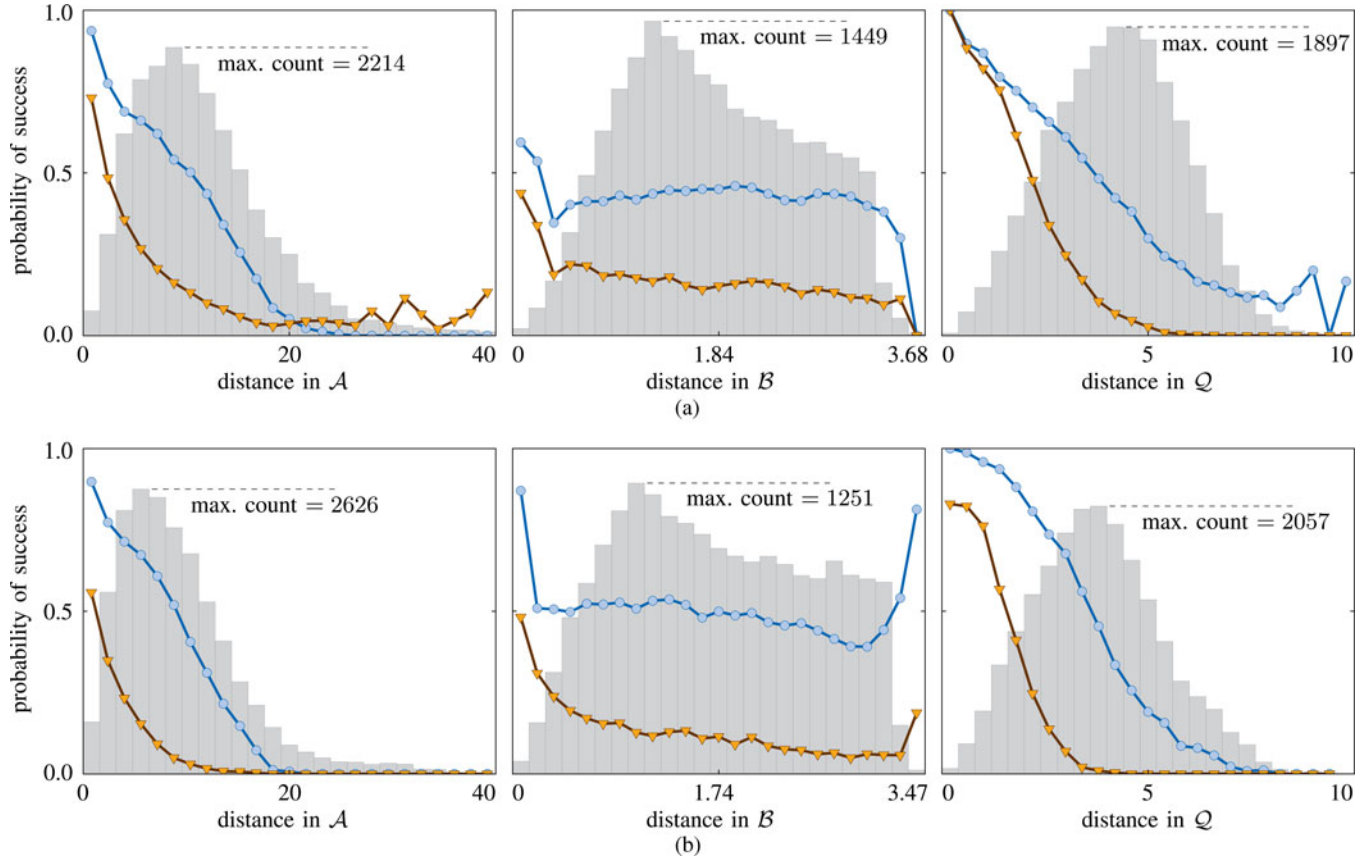

Fig. 5. Probability of successful local connection between randomly sampled points $a, a' \in \mathcal{A}_{\text{stable}}$ using straight-line paths in $\mathcal{A}$ (blue circles) and in $\mathcal{B}$ (orange triangles) as a function of distance for a chain with (a) $n = 4$ joints and (b) $n = 10$ joints. Results are shown with respect to distance measured in $\mathcal{A}$ (left), $\mathcal{B}$ (center), and $\mathcal{Q}$ (right). A histogram shows the induced distribution after 20 000 samples over each measure of distance. (a) Results for $n = 4$ joints. (b) Results for $n = 10$ joints.

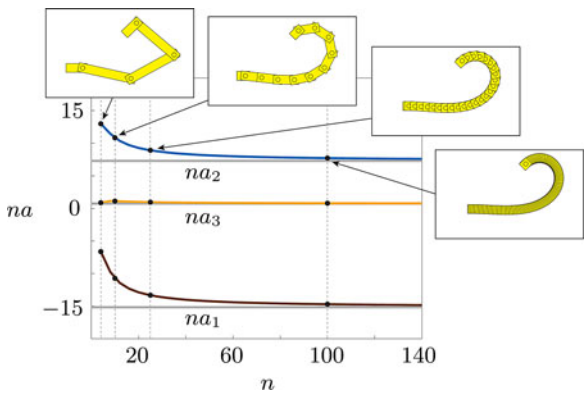

Fig. 6. To maintain fixed $b \in \mathcal{B}$ as n increases, the point $a \in \mathcal{A}$ must scale by a factor that approaches $1/n$ (asymptotes are shown as solid gray lines). The resulting configuration $\Psi(a) \in \mathcal{C}$ is shown in inset for $n = 4, 10, 25, 100$.

it is possible to establish asymptotic convergence of $\mathcal{A}_{\text{stable}}$ to a limiting set as n gets large. It will suffice to illustrate this convergence by example. In particular, Fig. 6 shows the result of holding $b \in \mathcal{B}$ constant, while increasing n. To maintain this boundary condition b, the point $a \in \mathcal{A}$ was required to scale by a factor that approached $1/n$. Moreover, the scaled point na converged to the initial costate (equivalently, the force and torque at the fixed base) that would have produced the limiting configuration $\Psi(a)$ in a continuum model of the chain. We will briefly describe such a model in Section V—it is the topic of ongoing work [51], [52].

C. On the Choice of Coordinates

Our approach to manipulation planning has been based on the knowledge that $\mathcal{A}$ is a valid choice of global coordinates with which to describe equilibrium configurations $\mathcal{C}_{\text{stable}} \subset \mathcal{C}$ of the chain. This result follows (by definition) from the diffeomorphism $\Psi : \mathcal{A} \to \mathcal{C}$. Readers familiar with numerical methods for optimal control may nevertheless remain concerned about our choice of coordinates and, in particular, about the sensitivity of this diffeomorphism—since we derived it by using an indirect method (i.e., by introduction of a costate trajectory), we expect that small perturbations about $a \in \mathcal{A}$ may give rise to large perturbations about $(u, x) = \Psi(a) \in \mathcal{C}$.

There are two reasons why this concern—which is motivated by our use of an indirect method—is somewhat misguided. First, we considered a discrete-time model (2) in this paper, and the distinction between indirect and direct methods of optimal control only makes sense in a continuous-time setting [62]. Second, were we to consider a continuous-time model (as we do in [51] and [52]), our approach to manipulation planning—with sampling and local connection in $\mathcal{A}$—would still not require

numerical solution of (2) for fixed b. Even local connection with straight-line paths in $\mathcal{B}$ (see Section III-D) would require only the computation of neighboring extremal solutions, for which indirect methods are well suited [55], [62].

However, there are also two reasons why the sensitivity of $\Psi(a)$ to perturbations about a should, indeed, concern us. First, sampling-based planning algorithms rely on accurate distance metrics for good performance. These metrics tell us, for example, when it is worthwhile to check if sampled points $a, a' \in \mathcal{A}_{\text{stable}}$ are $\mathcal{A}$-connected. Euclidean distance is a bad metric near points in $\mathcal{A}$ at which Ψ is highly sensitive. Second, robust implementation of planned paths in $\mathcal{A}_{\text{stable}}$ requires insensitivity of the equilibrium configuration (u, x) to changes in the gripper placement b. As we saw in Section III-D, it is equivalent that $\nabla_a(\Phi \circ \Psi|_{\mathcal{A}_{\text{stable}}})$ have a low condition number, a property that is directly related to the sensitivity of Ψ. As a heuristic, we might enforce an upper bound on the condition number of $\nabla_a(\Phi \circ \Psi|_{\mathcal{A}_{\text{stable}}})$ or sample more densely near points in $\mathcal{A}$ at which this condition number is high—we leave a full consideration of this problem to future work.

V. Conclusion

In this paper, we have looked at the problem of quasi-static manipulation planning for a kinematic chain with n joints that are linearly elastic torsional springs. What has made this problem seem hard in the past is the apparent lack of coordinates to describe equilibrium configurations. Our contribution was to show that the set of equilibrium configurations in this case is, in fact, a smooth three-manifold that can be parameterized globally by a single chart. This result allowed us to treat manipulation planning like any other motion planning problem—it produced a "configuration space" $\mathcal{A}$, a "collision checker" to test membership in the part $\mathcal{A}_{\text{stable}}$ of $\mathcal{A}$ that corresponds to equilibrium configurations, and a diffeomorphism that allowed us to "implement" paths in $\mathcal{A}_{\text{stable}}$ by paths of the gripper. We discussed several advantages of planning in $\mathcal{A}$, in particular showing through analysis and experiments that $\mathcal{A}_{\text{stable}}$ has favorable visibility properties compared with the space $\mathcal{B}_{\text{stable}}$ of boundary conditions.

We acknowledge that the chain is not necessarily a good model of any "real-world" object. Here, it served primarily to illustrate our new approach to manipulation planning. We chose it for this purpose because its basic structure should be familiar to any student of robotics and because equilibrium configurations could be described as local optima of a discrete-time optimal control problem (as opposed to continuous-time)—this second property allowed us to rely on well-known necessary and sufficient conditions for optimality [54], [55].

Our approach is not restricted to this choice of model, however. In [51] and [52], we extend our theoretical framework to analysis of "Euler's elastica" (which is a continuous analog of the chain we consider in this paper [63]) and to analysis of the Kirchhoff elastic rod (which is a generalization of Euler's elastica to a 3-D workspace [44] that has been used to model objects like flexible wire [2]). Equilibrium configurations of the elastica are local optima of the continuous-time optimal control problem

$$\begin{aligned} \underset{x,u}{\text{minimize}} \quad & \frac{1}{2}\int_{i=0}^{1} u^2\, dt \\ \text{subject to} \quad & \dot{x}_1 = \cos x_3 \\ & \dot{x}_2 = \sin x_3 \\ & \dot{x}_3 = u \\ & x(0) = 0, \qquad x(1) = b \end{aligned} \tag{12}$$

for some $b \in \mathcal{B}$. Application of Pontryagin's maximum principle produces results similar to what we derived in Section III for the chain (i.e., the space of all local optima is a smooth three-manifold). Equilibrium configurations of the rod are local optima of the geometric optimal control problem

$$\begin{aligned} \underset{q,u}{\text{minimize}} \quad & \frac{1}{2}\int_{0}^{1} \left(c_1 u_1^2 + c_2 u_2^2 + c_3 u_3^2\right) dt \\ \text{subject to} \quad & \dot{q} = q(u_1 X_1 + u_2 X_2 + u_3 X_3 + X_4) \\ & q(0) = e, \qquad q(1) = b \end{aligned} \tag{13}$$

where $c_1, c_2, c_3 > 0$ are parameters that weight components of bending and torsion, $q(t) \in SE(3)$, e is the identity element of $SE(3)$, and $\{X_1, \ldots, X_6\}$ is a basis for the Lie algebra of $SE(3)$. Again, results are similar to Section III (i.e., the space of all local optima is a smooth six-manifold), although the analysis in this case is considerably more involved and follows from Lie–Poisson reduction [64].

These extensions to our theoretical framework are being validated with preliminary hardware experiments. In [52], for example, we enable an industrial robot to manipulate a thin, flexible strip of metal, which we show is modeled well by Euler's elastica. Experiments like these suggest that our approach to manipulation planning may, indeed, have an impact on the motivational applications listed in Section I.

Before closing, we will briefly describe two other extensions of a similar nature that are the topic of ongoing work. The first extension shows by example that our approach is not restricted to elastic objects (or, at least, not to objects with purely elastic energy). The second extension relates to parameter identification, with potential application (for instance) to data-driven modeling and perception of surgical thread [39].

1) Gravity and Other External Forces: It may be possible to generalize our approach to deal with other applied forces. For example, assume that each link i has mass m_i, that joints are massless, and that gravity acts along the $-e_2$ axis of frame 0. The total potential energy in the chain is then

$$\sum_{i=0}^{n-1}\left(\frac{1}{2}u(i)^2 + m_i g\left(x_2(i) + \frac{r_i \sin x_3(i)}{2}\right)\right).$$

In the summation, the first term is the elastic energy in joint i as earlier (2), Section III-A and the second term is the energy due to gravity. We expect that analysis in this case would proceed exactly as in Section III, with similar results. Other applied forces that admit representation as the gradient of a potential might be incorporated in the same way. An apparently much

harder problem is presented by kinematic chains of arbitrary topology (e.g., branching or closed loop) and, in general, by forces arising from interaction between disparate links, as in protein models.

2) Calibration of Physical Parameters: We assumed that the torsional spring in each joint of the chain had unit modulus of elasticity. It is easy to relax this assumption; therefore, the total elastic energy becomes

$$\frac{1}{2}\sum_{i=0}^{n-1} c_i u(i)^2$$

for some set of parameters $c_0, \ldots, c_{n-1} > 0$. We might also allow each spring to have a nonzero bias, as in

$$\frac{1}{2}\sum_{i=0}^{n-1} (u(i) - c_i)^2$$

for some $c_0, \ldots, c_{n-1} \in \mathbb{R}$. In each case, analysis would again proceed exactly as in Section III. Although this extension is an easy one, it gives rise to the much more interesting problem of "calibration"—how do you infer what is the modulus (or the angular bias) at each joint? Finding these parameters from observations of equilibrium configurations can be cast as an inverse optimal control problem [39]. The structure established by Theorem 2 allows us to define a notion of orthogonal distance between $\mathcal{C}$ and these observations, similar to [65], and may lead to an efficient method of solution.

APPENDIX A
SMOOTH MANIFOLDS

Here, we recall basic definitions and state a useful fact about smooth (i.e., differentiable) manifolds [66].

A *topological n-manifold* $\mathcal{M}$ is a topological space that is Hausdorff, second countable, and locally Euclidean of dimension n. A *chart* on $\mathcal{M}$ is a pair $(\mathcal{U}, \alpha)$, where $\mathcal{U} \subset \mathcal{M}$ and $\alpha(\mathcal{U}) \subset \mathbb{R}^n$ are both open and where $\alpha : \mathcal{U} \to \alpha(\mathcal{U})$ is a homeomorphism. An *atlas* on $\mathcal{M}$ is a collection of charts whose domain covers $\mathcal{M}$. Two charts $(\mathcal{U}, \alpha)$ and $(\mathcal{V}, \Phi)$ on $\mathcal{M}$ are *smoothly compatible* if either $\mathcal{U}$ and $\mathcal{V}$ are disjoint or the composition $\Phi \circ \alpha^{-1}$ is a diffeomorphism (i.e., is a smooth function between open subsets of $\mathbb{R}^n$ that has a smooth inverse, where by "smooth" we mean in the class C^∞). A *smooth atlas* is an atlas in which any two charts are smoothly compatible. A chart that is part of a smooth atlas is called a *smooth chart*. A smooth atlas is *maximal* if it is not contained in any other strictly larger smooth atlas. A maximal smooth atlas is called a *smooth structure*. A *smooth n-manifold* is a topological n-manifold equipped with a smooth structure. It can be shown that any smooth atlas is contained in a unique maximal smooth atlas; therefore, to define a smooth n-manifold $\mathcal{M}$, it suffices only to specify some smooth atlas on $\mathcal{M}$. A map $f : \mathcal{M} \to \mathcal{N}$ between smooth manifolds $\mathcal{M}$ and $\mathcal{N}$ is a *smooth map* if for every $p \in \mathcal{M}$, there exist smooth charts $(\mathcal{U}, \alpha)$ on $\mathcal{M}$ and $(\mathcal{V}, \Phi)$ on $\mathcal{N}$ such that

$$p \in \mathcal{U}, \qquad f(p) \in \mathcal{V}, \qquad f(\mathcal{U}) \subset \mathcal{V} \tag{14}$$

and $\Phi \circ f \circ \alpha^{-1} : \alpha(\mathcal{U}) \to \Phi(\mathcal{V})$ is smooth. A *diffeomorphism* between smooth n-manifolds $\mathcal{M}$ and $\mathcal{N}$ is a smooth map $f : \mathcal{M} \to \mathcal{N}$ that is bijective and that has a smooth inverse.

We require the following result.

Lemma 3: If the topological n-manifold $\mathcal{M}$ has an atlas consisting of the single chart $(\mathcal{M}, \alpha)$, then $\mathcal{N} = \alpha(\mathcal{M})$ is a topological n-manifold with an atlas consisting of the single chart $(\mathcal{N}, \mathrm{id}_{\mathcal{N}})$, where $\mathrm{id}_{\mathcal{N}}$ is the identity map. Furthermore, both $\mathcal{M}$ and $\mathcal{N}$ are smooth n-manifolds and $\alpha : \mathcal{M} \to \mathcal{N}$ is a diffeomorphism.

Proof: Since $(\mathcal{M}, \alpha)$ is chart, $\mathcal{N}$ is an open subset of $\mathbb{R}^n$ and α is a bijection. Hence, our first result is immediate and our second result requires only that both α and α^{-1} are smooth maps. For every $p \in \mathcal{M}$, the charts $(\mathcal{M}, \alpha)$ and $(\mathcal{N}, \mathrm{id}_{\mathcal{N}})$ satisfy (14) and we have $\mathrm{id}_{\mathcal{N}} \circ \alpha \circ \alpha^{-1} = \mathrm{id}_{\mathcal{N}}$; therefore, α is a smooth map. For every $q \in \mathcal{N}$, the charts $(\mathcal{N}, \mathrm{id}_{\mathcal{N}})$ and $(\mathcal{M}, \alpha)$ again satisfy (14) and we have $\alpha \circ \alpha^{-1} \circ \mathrm{id}_{\mathcal{N}} = \mathrm{id}_{\mathcal{N}}$; therefore, α^{-1} is also a smooth map, and our result follows. ∎

APPENDIX B
PROOF THAT $\Psi : \mathcal{A} \to \mathcal{C}$ IS A HOMEOMORPHISM

Our main result in this section is Lemma 9, which is necessary in the proof of Theorem 2 in Section III-B. We will first prove five supporting lemmas.

Lemma 4: If $(u, x) = \Psi(a)$ and $p = \Gamma(a)$ for $a \in \mathbb{R}^3$, then

$$u(i) = -a_1 x_2(i+1) + a_2 x_1(i+1) - a_3$$

for $i \in \{0, \ldots, n-1\}$.

Proof: From (5), we compute

$$\begin{aligned} p_1(i+1) &= p_1(i) \\ p_2(i+1) &= p_2(i) \\ p_3(i+1) &= p_1(i)\,(x_2(i+1) - x_2(i)) \\ &\quad - p_2(i)\,(x_1(i+1) - x_1(i)) + p_3(i) \end{aligned}$$

for $i \in \{0, \ldots, n-1\}$. Since $x(0) = 0$ and $p(0) = a$, it is equivalent that

$$\begin{aligned} p_1(i) &= a_1 \\ p_2(i) &= a_2 \\ p_3(i) &= a_1 x_2(i) - a_2 x_1(i) + a_3 \end{aligned}$$

for $i \in \{0, \ldots, n\}$. We conclude that

$$\begin{aligned} u(i) &= -p(i+1)^T e_3 \\ &= -p_3(i+1) \\ &= -a_1 x_2(i+1) + a_2 x_1(i+1) - a_3 \end{aligned}$$

as desired. ∎

Lemma 5: A point (u, x) is regular with respect to (2) if and only if

$$u(i) \notin \{k\pi : k \in \mathbb{Z}\}$$

for some $i \in \{1, \ldots, n-2\}$.

Proof: The problem (2) has $3n+6$ equality constraints. By definition, a point (u,x) is regular with respect to these constraints if the corresponding gradient vectors are linearly independent [54]. By direct computation, it is equivalent that

$$\begin{bmatrix} 0 & 0 & \cdots & 0 & 0 & -I & 0 & \cdots & 0 & 0 \\ e_3 & 0 & \cdots & 0 & 0 & J_0 & -I & \cdots & 0 & 0 \\ 0 & e_3 & \cdots & 0 & 0 & 0 & J_1 & \cdots & 0 & 0 \\ \vdots & \vdots & \ddots & \vdots & \vdots & \vdots & \vdots & \ddots & \vdots & \vdots \\ 0 & 0 & \cdots & e_3 & 0 & 0 & 0 & \cdots & -I & 0 \\ 0 & 0 & \cdots & 0 & e_3 & 0 & 0 & \cdots & J_{n-1} & -I \\ 0 & 0 & \cdots & 0 & 0 & 0 & 0 & \cdots & 0 & I \end{bmatrix}$$

is full rank. By row reduction, it is equivalent that

$$\begin{bmatrix} (J_{n-1}\cdots J_1)\, e_3 & \cdots & J_{n-1}e_3 & e_3 \end{bmatrix} \tag{15}$$

is full rank. Matrix (15) is the manipulator Jacobian; therefore, (u,x) is regular if and only if it defines a nonsingular configuration of the kinematic chain. Nonsingular configurations are exactly those satisfying $u(i) \notin \{k\pi : k \in \mathbb{Z}\}$ for some $i \in \{1,\ldots,n-2\}$ (e.g., see [67]). ■

Lemma 6: Pick $a \in \mathbb{R}^3$, and let $(u,x) = \Psi(a)$. If for some $i \in \{0,\ldots,n-2\}$ there exist $m_i, m_{i+1} \in \mathbb{Z}$ such that $u(i) = m_i\pi$ and $u(i+1) = m_{i+1}\pi$, then $a \in \mathcal{S}$.

Proof: From (5) and Lemma 4, we compute

$$m_i\pi = u(i-1) - a_1 r_i \sin x_3(i) + a_2 r_i \cos x_3(i)$$

$$m_{i+1}\pi = m_i\pi + \cos m_i\pi \left(-a_1 r_i \sin x_3(i) + a_2 r_i \cos x_3(i)\right).$$

Solving, we find that

$$u(i-1) = (m_i \pm (m_i - m_{i+1}))\,\pi = m_{i-1}\pi$$

for some $m_{i-1} \in \mathbb{Z}$. By repeating this process, we find that $u(0) = m_0\pi$ and $u(1) = m_1\pi$ for some $m_0, m_1 \in \mathbb{Z}$. From (5), we compute

$$x(1) = \begin{bmatrix} 0 \\ 0 \\ m_0\pi \end{bmatrix} \quad \text{and} \quad x(2) = \begin{bmatrix} (n-1)^{-1}\cos(m_0\pi) \\ 0 \\ (m_0+m_1)\pi \end{bmatrix}.$$

By Lemma 4, we have

$$m_0\pi = u(0) = -a_3$$
$$m_1\pi = u(1) = a_2(n-1)^{-1}\cos(m_0\pi) - a_3.$$

Solving, we find that

$$a_2 = \pm(m_1 - m_0)(n-1)\pi$$
$$a_3 = -m_0\pi$$

hence that $a \in \mathcal{S}$. ■

Lemma 7: A point $\Psi(a)$ is regular with respect to (2) if and only if $a \in \mathcal{A}$.

Proof: We will prove the contrapositive that $(u,x) = \Psi(a)$ is not regular if and only if $a \in \mathcal{S} = \mathbb{R}^3 \backslash \mathcal{A}$. By Lemma 5, it is equivalent to show that $u(i) \in \{k\pi : k \in \mathbb{Z}\}$ for all $i \in \{1,\ldots,n-2\}$ if and only if $a \in \mathcal{S}$.

First, let $a \in \mathcal{S}$ and take $(u,x) = \Psi(a)$. We have

$$\begin{aligned} u(0) &= -a_3 && \text{(by Lemma 4)} \\ &\in \{k\pi : k \in \mathbb{Z}\} && \text{(by definition of } \mathcal{S}). \end{aligned}$$

For some $i \in \{1,\ldots,n-2\}$, assume $u(j) \in \{k\pi : k \in \mathbb{Z}\}$ for all $j \in \{0,\ldots,i-1\}$. From (5), it must also be true that $x_1(i+1) = m(n-1)^{-1}$ and $x_2(i+1) = 0$ for some $m \in \mathbb{Z}$. By Lemma 4 and the definition of $\mathcal{S}$, we conclude that

$$u(i) = a_2 m(n-1)^{-1} - a_3 = (km - l)\pi$$

for some $k, l \in \mathbb{Z}$, hence, that $u(i) \in \{k\pi : k \in \mathbb{Z}\}$. Our result proceeds by induction.

Now, let $a \in \mathbb{R}^3$, take $(u,x) = \Psi(a)$, and assume $u(i) \in \{k\pi : k \in \mathbb{Z}\}$ for all $i \in \{1,\ldots,n-2\}$. In particular, we have $u(1) = m_1\pi$ and $u(2) = m_2\pi$ for some $m_1, m_2 \in \mathbb{Z}$. By Lemma 6, $a \in S$. ■

Lemma 8: If $\Psi(a) = \Psi(a')$ for $a, a' \in \mathcal{A}$, then $a = a'$.

Proof: Suppose $(u,x) = \Psi(a)$ for some $a \in \mathcal{A}$. It suffices to show that a is uniquely determined by (u,x). From (5) and Lemma 4, we have

$$\begin{bmatrix} -r_i \sin x_3(i) & r_i \cos x_3(i) & 0 \\ -r_j \sin x_3(j) & r_j \cos x_3(j) & 0 \\ 0 & 0 & 1 \end{bmatrix} \begin{bmatrix} a_1 \\ a_2 \\ a_3 \end{bmatrix} = \begin{bmatrix} u(i) - u(i-1) \\ u(j) - u(j-1) \\ -u(0) \end{bmatrix} \tag{16}$$

for any $i, j \in \{0,\ldots,n-1\}$. By Lemma 7, (u,x) is regular. Hence, by Lemma 5, we can choose $i, j \in \{1,\ldots,n-2\}$ so that (16) admits a unique solution. Our result follows. ■

We are now ready to prove our main result.

Lemma 9: The map $\Psi : \mathcal{A} \to \mathcal{C}$ is a homeomorphism.

Proof: First, we will show that Ψ is a continuous bijection. By construction, $\Psi(a)$ satisfies (3) and (4) for the choice of costate $\Gamma(a)$, for any $a \in \mathbb{R}^3$. By Lemma 7, $\Psi(a)$ is regular if and only if $a \in \mathcal{A} \subset \mathbb{R}^3$. As a consequence, Ψ is both well defined and onto. Lemma 8 implies that Ψ is also one-to-one. Continuity of Ψ then follows immediately from (5).

It remains only to show that $\Psi^{-1} : \mathcal{C} \to \mathcal{A}$ is continuous. This result is a corollary to the proof of Lemma 8, since all quantities in (16) depend continuously on (u,x). ■

APPENDIX C
PROOF THAT ISSTABLE IS CORRECT

Our main result in this section is a proof of Theorem 4, which establishes correctness of the algorithm ISSTABLE (see Fig. 3) in Section III-C.

Proof of Theorem 4: Assume ISSTABLE(a) returns TRUE. Let $v_j(z)$ be the cost to go from $\delta x(j) = z$ in (9), for $j \in \{0,\ldots,n-1\}$. We have

$$v_{n-4}(z) = \min_y \left\{ \frac{1}{2}(y^T M y + z^T Q_{n-4} z) : Ay = Bz \right\} \tag{17}$$

where A, B, and M are as defined in Fig. 3 . The matrix A loses rank if and only if $u(n-3) = k\pi$ and $u(n-2) = l\pi$ for some $k, l \in \mathbb{Z}$, which by Lemma 6 contradicts our assumption that $a \in \mathcal{A}$; therefore, A is full rank. Hence, we can rewrite (17) as the quadratic form

$$v_{n-4}(z) = \min_y \left\{ \frac{1}{2}(A^\dagger Bz + Ny)^T M(A^\dagger Bz + Ny) + \frac{1}{2} z^T Q_{n-4} z \right\}.$$

Since $N^T MN > 0$ by assumption, we conclude that

$$v_{n-4}(z) = z^T P_{n-4} z$$

where the minimum is achieved by $y = -KA^\dagger Bz$. With a standard dynamic programming argument, we have

$$v_i(z) = \min_{\delta u(i)} \left\{ \frac{1}{2} \left(z^T Q_i z + \delta u(i)^2 \right) + v_{i+1} \left(J_i z + e_3 \delta u(i) \right) \right\} \tag{18}$$

for $i \in \{n-5, \ldots, 0\}$. If

$$v_{i+1}(z) = z^T P_{i+1} z$$

then since

$$s_{i+1} = 1 + e_3^T P_{i+1} e_3 > 0$$

by assumption, we conclude that

$$\begin{aligned} v_i(z) &= z^T \left(Q_i + J_i^T (P_{i+1} - P_{i+1} e_3 s_{i+1}^{-1} e_3^T P_{i+1}) J_i \right) z \\ &= z^T P_i z \end{aligned}$$

where the minimum is achieved by

$$\delta u(i) = -s_{i+1}^{-1} e_3^T P_{i+1} J_i z.$$

In particular, $v_0(z) = z^T P_0 z$ and $\delta u(0) = -s_1^{-1} e_3^T P_1 J_0 z$. Since we are given $\delta x(0) = 0$, we find that $\delta u(0) = 0$, hence, that $\delta x(1) = 0$ as well. Repeating this process, we see that (9) has unique solution $(\delta u, \delta x) = (0, 0)$; therefore, $a \in \mathcal{A}_{\text{stable}}$.

Now, assume IsStable(a) returns FALSE. If $N^T MN \not> 0$, then (17) is either unbounded below or admits multiple solutions for y, both of which imply that $a \notin \mathcal{A}_{\text{stable}}$. If $1 + e_3^T P_{i+1} e_3 \not> 0$ for some $i \in \{n-5, \ldots, 0\}$, then (18) is either unbounded below or admits multiple solutions for $\delta u(i)$, both of which again imply that $a \notin \mathcal{A}_{\text{stable}}$. These are the only two possibilities; therefore, we have our result. ■

ACKNOWLEDGMENT

The authors would like to thank S. Hutchinson for helpful discussions and K. Derosier, R. Morris-Wright, D. Shimamoto, and P. Walsh for many suggestions and for correction of several typographical errors. Lemma 8, in particular, was provided by D. Shimamoto.

REFERENCES

[1] F. Lamiraux and L. E. Kavraki, "Planning paths for elastic objects under manipulation constraints," *Int. J. Robot. Res.*, vol. 20, no. 3, pp. 188–208, 2001.
[2] M. Moll and L. E. Kavraki, "Path planning for deformable linear objects," *IEEE Trans. Robot.*, vol. 22, no. 4, pp. 625–636, Aug. 2006.
[3] J. E. Hopcroft, J. K. Kearney, and D. B. Krafft, "A case study of flexible object manipulation," *Int. J. Robot. Res.*, vol. 10, no. 1, pp. 41–50, 1991.
[4] J. Takamatsu, T. Morita, K. Ogawara, H. Kimura, and K. Ikeuchi, "Representation for knot-tying tasks," *IEEE Trans. Robot.*, vol. 22, no. 1, pp. 65–78, Feb. 2006.
[5] H. Wakamatsu, E. Arai, and S. Hirai, "Knotting/unknotting manipulation of deformable linear objects," *Int. J. Robot. Res.*, vol. 25, no. 4, pp. 371–395, 2006.
[6] M. Saha and P. Isto, "Manipulation planning for deformable linear objects," *IEEE Trans. Robot.*, vol. 23, no. 6, pp. 1141–1150, Dec. 2007.
[7] M. Bell and D. Balkcom, "Knot tying with single piece fixtures," in *Proc. Int. Conf. Robot. Autom.*, May 2008, pp. 379–384.
[8] J. van den Berg, S. Miller, D. Duckworth, H. Hu, A. Wan, X.-Y. Fu, K. Goldberg, and P. Abbeel, "Superhuman performance of surgical tasks by robots using iterative learning from human-guided demonstrations," in *Proc. Int. Conf. Robot. Autom.*, May 2010, pp. 2074–2081.
[9] H. Inoue and H. Inaba, "Hand-eye coordination in rope handling," in *Proc. Int. Symp. Robot. Res.*, 1985, pp. 163–174.
[10] M. Bell, "Flexible object manipulation" Ph.D. dissertation, Dept. Comput. Sci., Dartmouth College, Hanover, NH, Feb. 2010.
[11] J. van den Berg, S. Miller, K. Goldberg, and P. Abbeel, "Gravity-based robotic cloth folding," in *Proc. 9th Int. Workshop Algorithmic Found. Robot.*, 2011, pp. 409–424.
[12] Y. Yamakawa, A. Namiki, and M. Ishikawa, "Motion planning for dynamic folding of a cloth with two high-speed robot hands and two high-speed sliders," in *Proc. Int. Conf. Robot. Autom.*, May 2011, pp. 5486–5491.
[13] D. J. Balkcom and M. T. Mason, "Robotic origami folding," *Int. J. Robot. Res.*, vol. 27, no. 5, pp. 613–627, 2008.
[14] Y. Asano, H. Wakamatsu, E. Morinaga, E. Arai, and S. Hirai, "Deformation path planning for manipulation of flexible circuit boards," in *Proc. IEEE/RSJ Int. Conf. Intell. Robot. Syst.*, Oct. 2010, pp. 5386–5391.
[15] R. Jansen, K. Hauser, N. Chentanez, F. van der Stappen, and K. Goldberg, "Surgical retraction of non-uniform deformable layers of tissue: 2d robot grasping and path planning," in *Proc. IEEE/RSJ Int. Conf. Intell. Robot. Syst.*, Oct. 2009, pp. 4092–4097.
[16] Q. Lin, J. Burdick, and E. Rimon, "A stiffness-based quality measure for compliant grasps and fixtures," *IEEE Trans. Robot. Autom.*, vol. 16, no. 6, pp. 675–688, Dec. 2000.
[17] J.-S. Cheong, K. Goldberg, M. Overmars, and A. van der Stappen, "Fixturing hinged polygons," in *Proc. Int. Conf. Robot. Autom.*, 2002, vol. 1, pp. 876–881.
[18] K. Gopalakrishnan and K. Goldberg, "D-space and deform closure grasps of deformable parts," *Int. J. Robot. Res.*, vol. 24, no. 11, pp. 899–910, Nov. 2005.
[19] N. M. Amato and G. Song, "Using motion planning to study protein folding pathways," *J. Comput. Biol.*, vol. 9, no. 2, pp. 149–168, 2002.
[20] M. S. Apaydin, D. L. Brutlag, C. Guestrin, D. Hsu, J.-C. Latombe, and C. Varma, "Stochastic roadmap simulation: An efficient representation and algorithm for analyzing molecular motion," *J. Comput. Biol*, vol. 10, no. 3–4, pp. 257–281, 2003.
[21] J. Cortés, T. Siméon, M. Remaud-Siméon, and V. Tran, "Geometric algorithms for the conformational analysis of long protein loops," *J. Comput. Chem.*, vol. 25, no. 7, pp. 956–967, 2004.
[22] M. L. Teodoro, G. N. Phillips, and L. E. Kavraki, "Understanding protein flexibility through dimensionality reduction," *J. Comput. Biol.*, vol. 10, no. 3–4, pp. 617–634, 2004.
[23] H. Tanner, "Mobile manipulation of flexible objects under deformation constraints," *IEEE Trans. Robot.*, vol. 22, no. 1, pp. 179–184, Feb. 2006.
[24] G. S. Chirikjian and J. W. Burdick, "The kinematics of hyper-redundant robot locomotion," *IEEE Trans. Robot. Autom.*, vol. 11, no. 6, pp. 781–793, Dec. 1995.
[25] M. W. Hannan and I. D. Walker, "Kinematics and the implementation of an elephant's trunk manipulator and other continuum style robots," *J. Robot. Syst.*, vol. 20, no. 2, pp. 45–63, 2003.
[26] B. A. Jones and I. D. Walker, "Kinematics for multisection continuum robots," *IEEE Trans. Robot.*, vol. 22, no. 1, pp. 43–55, Feb. 2006.
[27] D. B. Camarillo, C. F. Milne, C. R. Carlson, M. R. Zinn, and J. K. Salisbury, "Mechanics modeling of tendon-driven continuum

manipulators," *IEEE Trans. Robot.*, vol. 24, no. 6, pp. 1262–1273, Dec. 2008.
[28] D. C. Rucker, R. J. Webster, G. S. Chirikjian, and N. J. Cowan, "Equilibrium conformations of concentric-tube continuum robots," *Int. J. Robot. Res.*, vol. 29, no. 10, pp. 1263–1280, 2010.
[29] R. J. Webster and B. A. Jones, "Design and kinematic modeling of constant curvature continuum robots: A review," *Int. J. Robot. Res.*, vol. 29, no. 13, pp. 1661–1683, 2010.
[30] Y. Nakamura, *Advanced Robotics: Redundancy and Optimization*. Reading, MA: Addison-Wesley, 1991.
[31] A. Shkolnik and R. Tedrake, "Path planning in 1000+ dimensions using a task-space Voronoi bias," in *Proc. Int. Conf. Robot. Autom.*, Kobe, Japan, May 2009, pp. 2061–2067.
[32] M. Behnisch, R. Haschke, and M. Gienger, "Task space motion planning using reactive control," in *Proc. IEEE/RSJ Int. Conf. Intell. Robot. Syst.*, Oct. 2010, pp. 5934–5940.
[33] G. Chirikjian and J. Burdick, "A modal approach to hyper-redundant manipulator kinematics," *IEEE Trans. Robot. Autom.*, vol. 10, no. 3, pp. 343–354, Jun. 1994.
[34] A. De Luca and G. Oriolo, "Nonholonomic behavior in redundant robots under kinematic control," *IEEE Trans. Robot. Autom.*, vol. 13, no. 5, pp. 776–782, Oct. 1997.
[35] A. De Luca, R. Mattone, and G. Oriolo, "Steering a class of redundant mechanisms through end-effector generalized forces," *IEEE Trans. Robot. Autom.*, vol. 14, no. 2, pp. 329–335, Apr. 1998.
[36] O. Khatib, "A unified approach for motion and force control of robot manipulators: The operational space formulation," *IEEE J. Robot. Autom.*, vol. RA-3, no. 1, pp. 43–53, Feb. 1987.
[37] Z. McCarthy and T. Bretl, "Mechanics and manipulation of planar elastic kinematic chains," in *Proc. IEEE Int. Conf. Robot. Autom.*, St. Paul, MN, May 2012, pp. 2798–2805.
[38] M. Bergou, M. Wardetzky, S. Robinson, B. Audoly, and E. Grinspun, "Discrete elastic rods," *ACM Trans. Graph.*, vol. 27, no. 3, pp. 1–12, 2008.
[39] S. Javdani, S. Tandon, J. Tang, J. F. O'Brien, and P. Abbeel, "Modeling and perception of deformable one-dimensional objects," presented at the Int. Conf. Robot. Autom., Shanghai, China, May 2011.
[40] J. Langer and D. Singer, "The total squared curvature of closed curves," *J. Diff. Geom.*, vol. 20, pp. 1–22, 1984.
[41] J. Langer and D. A. Singer, "Lagrangian aspects of the Kirchhoff elastic rod," *SIAM Rev.*, vol. 38, no. 4, pp. 605–618, 1996.
[42] G. Walsh, R. Montgomery, and S. Sastry, "Optimal path planning on matrix lie groups," in *Proc. IEEE Conf. Decis. Control*, Dec. 1994, vol. 2, pp. 1258–1263.
[43] V. Jurdjevic, *Integrable Hamiltonian Systems on Complex Lie Groups*. vol. 838, Providence, RI: Amer. Math. Soc., 2005.
[44] J. Biggs, W. Holderbaum, and V. Jurdjevic, "Singularities of optimal control problems on some 6-d Lie groups," *IEEE Trans. Autom. Control*, vol. 52, no. 6, pp. 1027–1038, Jun. 2007.
[45] Y. Sachkov, "Maxwell strata in the Euler elastic problem," *J. Dyn. Control Syst.*, vol. 14, no. 2, pp. 169–234, 2008.
[46] Y. Sachkov, "Conjugate points in the Euler elastic problem," *J. Dyn. Control Syst.*, vol. 14, no. 3, pp. 409–439, 2008.
[47] T. A. Ivey and D. A. Singer, "Knot types, homotopies and stability of closed elastic rods," *Proc. Lond. Math. Soc.*, vol. 79, no. 2, pp. 429–450, 1999.
[48] S. Neukirch and M. Henderson, "Classification of the spatial equilibria of the clamped elastica: Symmetries and zoology of solutions," *J. Elasticity*, vol. 68, no. 1, pp. 95–121, 2002.
[49] M. E. Henderson and S. Neukirch, "Classification of the spatial equilibria of the clamped elastica: Numerical continuation of the solution set," *Int. J. Bifurcat. Chaos Appl. Sci. Eng.*, vol. 14, no. 4, pp. 1223–1239, 2004.
[50] S. S. Antman, *Nonlinear Problems of Elasticit*, (Applied Mathematical Sciences Series), vol. 107, 2nd ed. New York: Springer-Verlag, 2005.
[51] T. Bretl and Z. McCarthy, "Equilibrium configurations of a Kirchhoff elastic rod under quasi-static manipulation," presented at the Workshop Algorithmic Found. Robot., Boston, MA, Jun. 2012.
[52] D. Matthews and T. Bretl, "Experiments in quasi-static manipulation of a planar elastic rod," presented at the IEEE/RSJ Int. Conf. Intell. Robots Syst., 2012, to be published.
[53] D. K. Pai, "Strands: Interactive simulation of thin solids using Cosserat models," *Comput. Graph. Forum*, vol. 21, no. 3, pp. 347–352, 2002.
[54] D. G. Luenberger and Y. Ye, *Linear and Nonlinear Programmin* (Int. Series Operations Res. Manage. Sci.). vol. 116, 3rd ed. New York: Springer-Verlag, 2007.
[55] A. E. Bryson and Y.-C. Ho, *Applied Optimal Control*. Bristol, PA: Hemisphere, 1975.
[56] M. W. Spong, S. Hutchinson, and M. Vidyasagar, *Robot Modeling and Control*. New York: Wiley, 2006.
[57] J.-C. Latombe, *Robot Motion Planning*. Boston, MA: Kluwer, 1991.
[58] H. Choset, K. Lynch, S. Hutchinson, G. Kanto, W. Burgard, L. Kavraki, and S. Thrun, *Principles of Robot Motion: Theory, Algorithms, and Implementations*. Cambridge, MA: MIT Press, 2005.
[59] S. M. LaValle, *Planning Algorithms*. New York: Cambridge Univ. Press, 2006.
[60] L. E. Kavraki, P. Svetska, J.-C. Latombe, and M. Overmars, "Probabilistic roadmaps for path planning in high-dimensional configuration spaces," *IEEE Trans. Robot. Autom.*, vol. 12, no. 4, pp. 566–580, Aug. 1996.
[61] G. Sánchez and J.-C. Latombe, "On delaying collision checking in PRM planning: Application to multi-robot coordination," *Int. J. Robot. Res.*, vol. 21, no. 1, pp. 5–26, 2002.
[62] J. T. Betts, *Practical Methods for Optimal Control and Estimation Using Nonlinear Programming*, 2nd ed. Philadelphia, PA: SIAM, 2010.
[63] C. Truesdell, "The influence of elasticity on analysis: The classic heritage," *Bull. Amer. Math. Soc.*, vol. 9, pp. 293–310, 1983.
[64] J. E. Marsden and T. S. Ratiu, *Introduction to Mechanics and Symmetry: A Basic Exposition of Classical Mechanical Systems*, 2nd ed. New York: Springer-Verlag, 1999.
[65] A. Keshavarz, Y. Wang, and S. Boyd, "Imputing a convex objective function," in *Proc. IEEE Multi-Conf. Syst. Control*, Sep. 2011, pp. 613–619.
[66] J. M. Lee, *Introduction to Smooth Manifolds*. vol. 218, New York: Springer-Verlag, 2003.
[67] J. Trinkle and R. Milgram, "Complete path planning for closed kinematic chains with spherical joints," *Int. J. Robot. Res.*, vol. 21, no. 9, pp. 773–789, 2002.

Timothy Bretl (S'02–M'05) received the B.S. degree in engineering and the B.A. degree in mathematics from Swarthmore College, Swarthmore, PA, in 1999 and the M.S. and Ph.D. degrees both in aeronautics and astronautics from Stanford University, Stanford, CA, in 2000 and 2005, respectively.

Subsequently, he was a Postdoctoral Fellow with the Department of Computer Science, Stanford University. Since 2006, he has been with the University of Illinois at Urbana-Champaign, where he is currently an Assistant Professor of aerospace engineering with an affiliate appointment in the Coordinated Science Laboratory.

Dr. Bretl received the National Science Foundation Faculty Early Career Development Award in 2010.

Zoe McCarthy (S'12) received the B.S. degree in electrical and computer engineering from the University of Illinois at Urbana-Champaign in 2012. Since then, she has been a graduate student in the Department of Electrical Engineering and Computer Sciences, University of California at Berkeley.